lack NELL2 and are also partially deficient in the receptor Robo3 (while remaining excluded in mice that either lack NELL2 or partially lack Robo3 in isolation), implying that the NELL2 signaling pathway collaborates with others to ensure avoidance of the motor column. Our results also show that Robo3.1 serves as an integrative hub: Its three diverse actions in response to three different cues—mediating NELL2 repulsion from the motor column, potentiating midline Netrin-1 attraction, and antagonizing midline Slit repulsion—act simultaneously, are mutually reinforcing, and serve the common purpose of steering commissural axons toward and across the midline. This multiplicity of mechanisms likely helps ensure high-fidelity steering of axons to their targets.

REFERENCES AND NOTES

1. A. L. Kolodkin, M. Tessier-Lavigne, *Cold Spring Harb. Perspect. Biol.* **3**, a001727 (2011).
2. B. J. Dickson, Y. Zou, *Cold Spring Harb. Perspect. Biol.* **2**, a002055 (2010).
3. T. E. Kennedy, T. Serafini, J. R. de la Torre, M. Tessier-Lavigne, *Cell* **78**, 425–435 (1994).
4. H. Long *et al.*, *Neuron* **42**, 213–223 (2004).
5. Y. Zou, E. Stoeckli, H. Chen, M. Tessier-Lavigne, *Cell* **102**, 363–375 (2000).
6. R. Shirasaki, R. Katsumata, F. Murakami, *Science* **279**, 105–107 (1998).
7. B. J. Dickson, G. F. Gilestro, *Annu. Rev. Cell Dev. Biol.* **22**, 651–675 (2006).
8. A. Jaworski, H. Long, M. Tessier-Lavigne, *J. Neurosci.* **30**, 9445–9453 (2010).
9. K. Brose *et al.*, *Cell* **96**, 795–806 (1999).
10. L. Camurri *et al.*, *Mol. Cell. Neurosci.* **30**, 485–493 (2005).
11. E. T. Mambetisaeva, W. Andrews, L. Camurri, A. Annan, V. Sundaresan, *Dev. Dyn.* **233**, 41–51 (2005).
12. C. Sabatier *et al.*, *Cell* **117**, 157–169 (2004).
13. P. Zelina *et al.*, *Neuron* **84**, 1258–1272 (2014).
14. Z. Chen, B. B. Gore, H. Long, L. Ma, M. Tessier-Lavigne, *Neuron* **58**, 325–332 (2008).
15. S. R. Ramani *et al.*, *Anal. Biochem.* **420**, 127–138 (2012).
16. P. C. G. Haddick *et al.*, *PLOS ONE* **9**, e84823 (2014).
17. S. Matsuhashi *et al.*, *Dev. Dyn.* **203**, 212–222 (1995).
18. T. K. Watanabe *et al.*, *Genomics* **38**, 273–276 (1996).
19. Y. Jiang *et al.*, *Mol. Cell. Neurosci.* **41**, 113–119 (2009).
20. T. Serafini *et al.*, *Cell* **78**, 409–424 (1994).

ACKNOWLEDGMENTS

We thank the members of the Tessier-Lavigne laboratory for discussion and suggestions. We are grateful to C. Culiat for sharing *NELL1* mutant mice, J. Ernst for help with purification of recombinant proteins, S. Warming for advice on the assembly of the *NELL2* targeting vector by recombineering, M. Roose-Girma for help with generation of *NELL2* mutant mice, and M. Yaylaoglu for providing probe templates for in situ hybridization. The *NELL2* conditional and full knockout mice as well as cDNA constructs described here are available from A.J. under a material transfer agreement with Genentech. We also thank N. Velarde, D. Collado, K. Sono, and Y. Zhou for technical assistance. This work was supported by Genentech, The Rockefeller University, and Brown University. The supplementary materials contain additional data. Roche provided part of the support for the study but does not stand to benefit from it because no patents were filed.

SUPPLEMENTARY MATERIALS

www.sciencemag.org/content/350/6263/961/suppl/DC1
Materials and Methods
Figs. S1 to S4
Table S1
References (*21*–*27*)

17 August 2015; accepted 16 October 2015
10.1126/science.aad2615

CAMOUFLAGE

Open-ocean fish reveal an omnidirectional solution to camouflage in polarized environments

Parrish C. Brady,[1] Alexander A. Gilerson,[2] George W. Kattawar,[3] James M. Sullivan,[4] Michael S. Twardowski,[4] Heidi M. Dierssen,[5] Meng Gao,[3] Kort Travis,[1] Robert Ian Etheredge,[1] Alberto Tonizzo,[2] Amir Ibrahim,[2] Carlos Carrizo,[2] Yalong Gu,[2] Brandon J. Russell,[5] Kathryn Mislinski,[1] Shulei Zhao,[1] Molly E. Cummings[1]

Despite appearing featureless to our eyes, the open ocean is a highly variable environment for polarization-sensitive viewers. Dynamic visual backgrounds coupled with predator encounters from all possible directions make this habitat one of the most challenging for camouflage. We tested open-ocean crypsis in nature by collecting more than 1500 videopolarimetry measurements from live fish from distinct habitats under a variety of viewing conditions. Open-ocean fish species exhibited camouflage that was superior to that of both nearshore fish and mirrorlike surfaces, with significantly higher crypsis at angles associated with predator detection and pursuit. Histological measurements revealed that specific arrangements of reflective guanine platelets in the fish's skin produce angle-dependent polarization modifications for polarocrypsis in the open ocean, suggesting a mechanism for natural selection to shape reflectance properties in this complex environment.

Perhaps more than any other environment on Earth, the nature of the open ocean greatly limits camouflage strategies. The absence of objects to hide behind or against requires cryptic animals to blend into a background that is in constant flux. Open-ocean visual backgrounds result from light scattering off of water molecules and microscopic particles, and early characterizations suggested that this background was temporally variable (due to changes in water composition) but spatially uniform [symmetrical in the horizontal plane with a predictable vertical intensity gradient (*1*)]. Early theories proposed that the silvery sides of open-ocean fish evolved to mirror spatially homogeneous backgrounds (*2*–*5*) (figs. S1 and S2). This theory aligned with laboratory measurements showing more specular (mirrorlike) reflectance in open-ocean species and more diffuse (optically random) reflectance in their coastal counterparts (*6*). Recent research has unveiled an additional feature of light-scattering processes in open oceans that creates spatially heterogeneous backgrounds. Specifically, polarization (the directional vibration of light waves) generates changes in the light environment that vary with the Sun's position in the sky (*7*–*11*). The angular variability of the polarized light field creates an environment where fish encounter different polarization fields in every direction. Under these conditions, mirrors are expected to be highly detectable to organisms with polarization-sensitive vision (*12*) (movies S1 and S2). Because the ability to detect polarized light is common across diverse fish families (*13*–*15*), natural selection is likely to influence the evolution of fish reflectance properties to address this dynamic heterogeneity.

Comparative measurements in the laboratory hint at adaptive differences in polarized reflectance between fish from distinct habitats. Measurements from an open-ocean fish (the lookdown, *Selene vomer*) reveal polarized reflectance properties that change based on incident polarization, whereas pinfish (*Lagodon rhomboides*) living in depolarized nearshore environments show no polarization-dependent reflectance (*12*). Lookdowns appear to alter their polarized reflection properties to match the change in background as the Sun changes position in the sky (*12*) (movie S3). Evidence for polarized reflectance modulation has been found in multiple open-ocean species (*16*, *17*). Although these laboratory studies intriguingly suggest adaptations for camouflage, they cannot emulate the heterogeneity of natural light fields, and the ultimate test of crypsis must be conducted in the field.

[1]Department of Integrative Biology, University of Texas, Austin, TX 78712, USA. [2]Optical Remote Sensing Laboratory, the City College of New York–CUNY, New York, NY 10031, USA. [3]Department of Physics and Astronomy and Institute for Quantum Science and Engineering, Texas A&M University, College Station, TX 77843-4242, USA. [4]Harbor Branch Oceanographic Institute, Florida Atlantic University, Ft. Pierce, FL 34946, USA. [5]Department of Marine Sciences, University of Connecticut Avery Point, 1080 Shennecossett Road, Groton, CT 06340-6048, USA.

To empirically determine whether open-ocean fish have evolved a cryptic reflectance strategy for their heterogeneous polarized environment, we measured the contrasts of live open-ocean and coastal fish against the pelagic background in the Florida Keys and Curaçao. We tested whether open-ocean fish exhibit significantly lower contrast to their natural background [as measured by the Stokes contrast, *S*, which combines measures of polarization and intensity (fig. S3)] than fish that live in habitats with depolarized light. As a basis for comparison, we also tested whether open-ocean fish show lower contrast than previously proposed oceanic reflectance strategies (specular or diffuse mirror surfaces). Simultaneous videopolarimetry measurements from targets (fish and mirror surfaces) and water backgrounds were collected 2 to 4 m below the surface in deep open-ocean water (25 to 32 m depth) under a suite of solar elevation, predator (camera) viewing, and target positioning angles approximating an omnidirectional measurement (Fig. 1, movie S3, and supplementary materials and methods S1 and S2).

Field measurements verified the horizontal heterogeneity of the near-surface open-ocean polarized light environment (Fig. 1, D and E). A single 360° camera rotation around the horizontal plane of the target (azimuthal rotation) revealed that background intensity and degree of polarization varied by a factor >2, with the angle of polarization varying over 60° (Fig. 1E). Open-ocean species from the Carangidae fish family (lookdowns and bigeye scad, *Selar crumenophthalmus*) exhibited significantly lower contrast across viewing, solar, and target positioning angles than did carangid species inhabiting reef environments (bar jack, *Caranx ruber*; and almaco jack, *Seriola rivoliana*; Fig. 2 and table S1). Furthermore, open-ocean carangid fish revealed significantly lower contrasts than mirror surfaces, whereas reef-dwelling carangids showed significantly higher contrast than mirrors, and surface-skimming fish (ballyhoo, *Hemiramphus brasiliensis*) showed no difference (Fig. 2, A to E, figs. S4 to S6, and tables S2 to S9). The absence of fish polarocrypsis in reef environments is expected because of the depolarizing effects of the ocean floor (*18*), whereas a mirrorlike strategy may be sufficient for camouflage in the surface-skimming (<0.2 m) habitat of the ballyhoo, where the polarized field is chaotic (*19*).

The lower omnidirectional contrast of carangids that occupy open-ocean habitats suggests that their surface properties are subject to selection for camouflage. If natural selection is shaping fish reflectance, then we expect to find significant differences at viewing angles that are relevant for foraging and survival. Many carangid fish are piscivores (*20*, *21*), requiring a stealthy approach to prey while minimizing detection from predators. Fish predation is biased around a ~90° cone centered on the prey's tail (*22*), and mirrors produce strong polarized reflections at these obtuse, predatory "chase angles" (±45° from tail or head). Restricting our crypsis evaluation to chase angles only, we found that open-ocean carangid fish exhibit nearly twice the crypsis performance as nearshore carangids (table S1), and that these open-ocean species exhibited significantly lower contrasts than did mirror surfaces, whereas fish from other habitats did not (Figs. 2, F to J, and 3A and tables S2 and S6).

Although fish from open-ocean environments were more cryptic than our test surfaces (specular or diffuse mirrors) in nearly 75% of all chase-angle measurements from the field (Figs. 3A and 4A), we identified additional viewing angles in which these fish exhibit exceptional camouflage. Open-ocean carangids showed significantly lower contrast than mirrors or diffuse surfaces when viewed from above [camera inclination angle (θ_C) < −10°; Figs. 3B and 4B, fig. S6, and tables S2 and S5] or positioned directly orthogonal to a

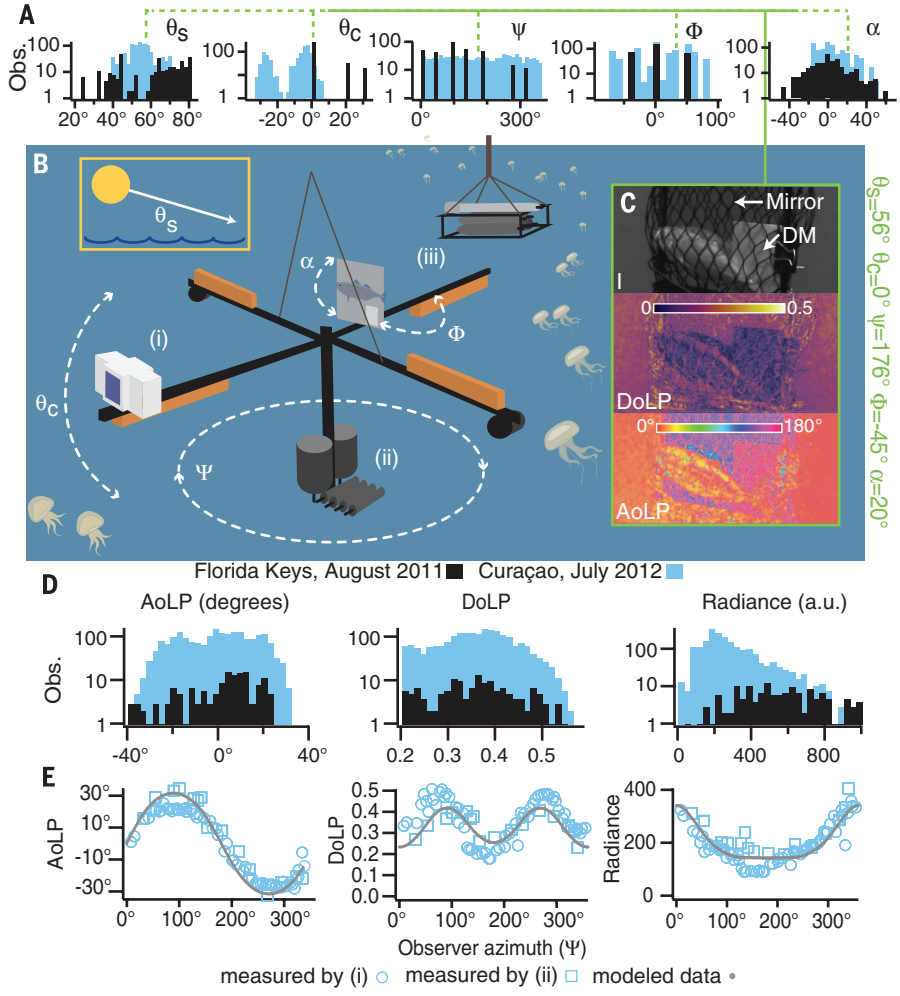

Fig. 1. Field measurement apparatus and angular configurations. (**A**) More than 1500 measurements collected at different angular configurations of solar angle (θ_s), camera inclination angle (θ_c), camera azimuth angle (ψ), relative yaw angle (φ), and fish pitch angle (α) from the Florida Keys (black) and Curaçao (blue). (**B**) Measurements were obtained with a (i) videopolarimeter using a remotely operated underwater rotating platform (supplementary materials and methods S1 and S2 and movie S3) and validated by measurements with (ii) a hyperspectral radiometric polarimeter and (iii) inherent optical properties simultaneously recorded [e.g., volume-scattering function measurements with the Multi-Angle Scattering Optical Tool (MASCOT)]. In Curaçao, integrated digital compass and inertial sensors with the videopolarimeter provided nearly continuous azimuth (ψ) and pitch (θ_c) angle measurements. (**C**) Polarimetric image of a bigeye scad restrained against mirror and diffuse mirror (DM), shown in radiance (or intensity, I), degree of linear polarization (DoLP), and angle of linear polarization (AoLP). (**D**) Azimuthal (ψ) background measurements of the water column AoLP, DoLP, and radiance in Curaçao (blue) and Florida (black). (**E**) Measurements and simulations of the background light field for a single azimuthal rotation (3 min) on 7 July 2012 in Curaçao (measured 2.5 m below the surface in 26.5 m of ocean depth; supplementary materials and methods S2 and table S10).

predator viewer in the horizontal plane (detection angles, where the fish flank is perfectly perpendicular to the predator's view, fish yaw $\phi = 0° \pm 10°$; Figs. 3A and 4C and tables S2 and S5). Furthermore, open-ocean fish showed significant increases in crypsis when the Sun was moderately high in the sky (solar altitude > 54%, Fig. 3C), as well as when potential predators were facing away from the Sun [camera azimuth angle (ψ) = 120° to 240°, Fig. 3D].

In order to understand the structural mechanism underlying this superior polarocrypsis in open-ocean fish, we evaluated fish skin properties in the laboratory with scanning electron microscopy (SEM), light microscopy, and whole-body videopolarimetry measurements. We found that the specific orientation of the fish's guanine platelets allows these open-ocean carangids to blend into the consistent vertical intensity profile of the open ocean, while also providing them the ability to blend into variable polarized backgrounds. Specifically, SEM measurements revealed that the open-ocean carangids have guanine platelets that are well aligned in a vertical plane (e.g., θ_G guanine platelet roll angles exhibit a narrow angular distribution; Fig. 4D and fig. S1, C and D) (*16*), which produces more specular reflection in the vertical direction and allows fish to match the predictable downward direction of light intensity in the open ocean. Meanwhile, the short axes of these guanine platelets have a very broad angular distribution (ϕ_G or yaw, Fig. 4D), which will result in greater diffuse intensity reflection along the horizontal axis [fig. S1M; similarly found in other silvery fish (*23*)]. This broad angular distribution in the horizontal plane may contribute to polarocrypsis by averaging the reflected light across a variable polarization background. Using both light microscopy and full-body videopolarimetry, we showed that the arrangement of guanine platelets produces two larger optical axes at the level of the whole fish (bulk reflectance; supplementary materials and methods S3 and Fig. 4E). These axes are roughly aligned with the anterior-posterior and dorsal-ventral axes of the fish (Fig. 4E). Full-body polarimetry measures of these fish in the lab confirm that these two axes have different polarization properties (see supplementary materials and methods S3 for in-depth results and discussion) that produce different polarization reflectance with different incident polarization light fields. Specifically, these two optical axes are responsible for the incident-specific polarization reflectance that open-ocean carangids exhibit, because this surface will reflect fully preserved polarized light when the incident polarization angles align with one of these axes, and will reflect depolarized light when incident light is misaligned with either axis. This specific arrangement probably accounts for the improved crypsis ability relative to mirror surfaces at azimuth viewing angles such as (120° to 240° in Fig. 3D, where carangid fish surfaces will convert incident polarized light into lower-degree horizontally polarized light matching the background (fig. S7), whereas mirror surfaces, with angle-invariant reflection, will not.

Our in-field evaluation shows that polarocryptic open-ocean fish address crypsis with omnidirectional solutions. Polarocryptic fish not only reduce the conspicuous polarized reflections associated with mirrorlike surfaces but also exhibit angle-specific polarization reflective properties that are particularly honed for crypsis from viewing angles under natural selection (predatory chase and detection angles). Their context-dependent reflectance strategy surpasses both traditional devices [mirrors (*24*)] and modern

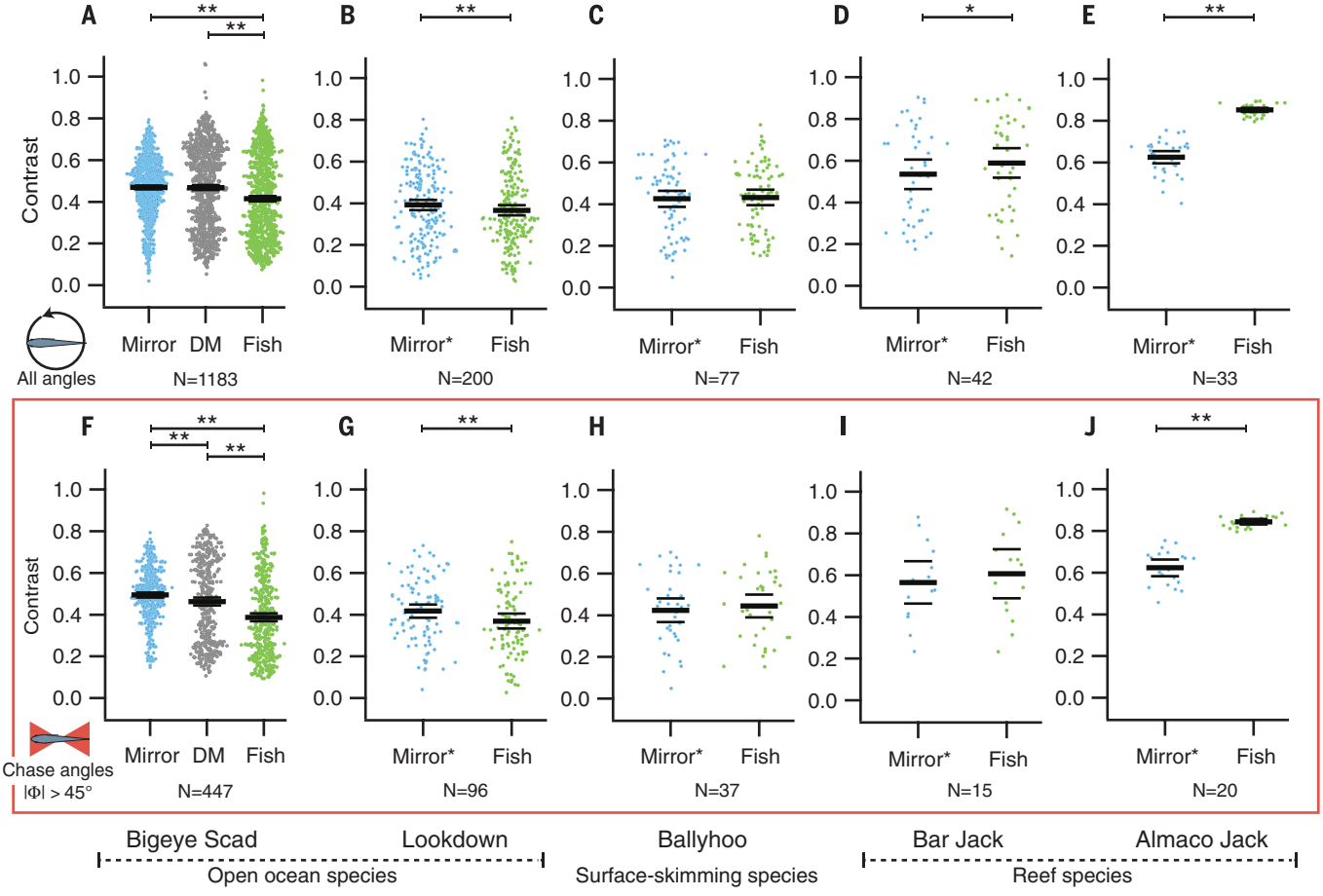

Fig. 2. Open-ocean fish species outperform nearshore fish and mirrored surfaces in epipelagic crypsis. (**A** to **E**) Videopolarmetric measurements of different species of silvery fish (green); specular mirror (mirror, blue), specular Mylar (mirror*, blue), and diffuse mirror (DM, gray) were evaluated in terms of *S* to the background environment (bigeye scad were measured in Curaçao; other fish were measured in Florida at 2 to 4 m below the surface in waters >25 m deep) in blue wavelengths with a 470-nm peak. (**F** to **J**) Measurements collected within chase angles only ($|\Phi| \geq 45°$). Averages and standard errors are denoted by black bars; statistical significant differences are denoted by * ($P < 0.05$) and ** ($P << 0.01$) (tables S2 to S9 and figs. S4 to S6).

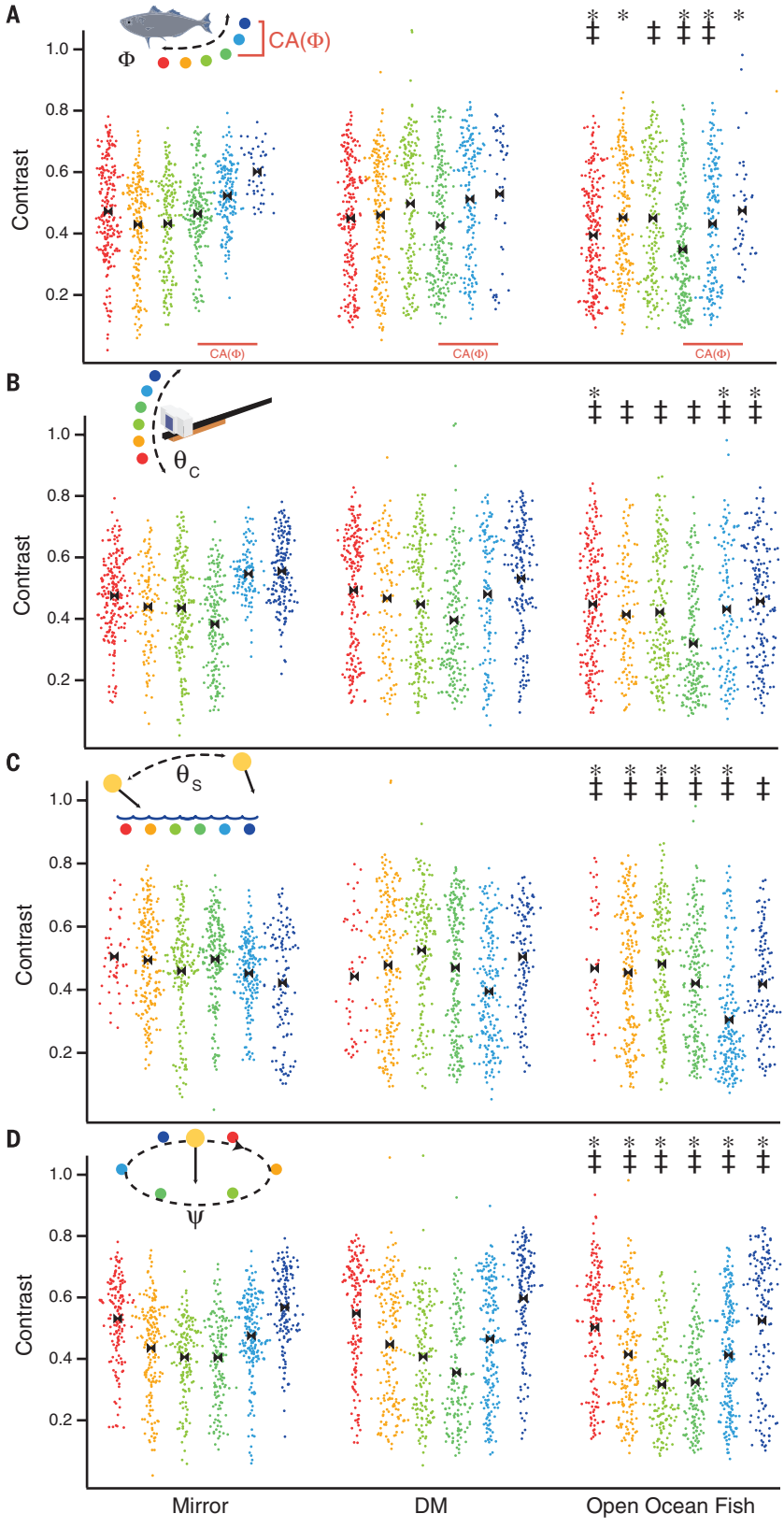

Fig. 3. Fine-scale evaluation of crypsis for the bigeye scad under different solar and viewing angles. Partitioning of the *S* distributions of Fig. 2A. Each color corresponds to a particular angular interval bin, and the averages of each bin are marked on each distribution in black. Significant differences (found through *t* tests) between fish and specular mirror distributions are denoted by *, and significant differences between the fish and diffuse mirror distributions are denoted by ‡. (**A**) Contrast distributions by absolute value of the relative yaw angle, ϕ, with specific ϕ bins of red: $0° < \phi \leq 15°$, orange: $15° < \phi \leq 30°$, light green: $30° < \phi \leq 45°$, green: $45° < \phi \leq 60°$, light blue: $60° < \phi \leq 75°$, and blue: $75° < \phi \leq 90°$. (**B**) Contrast distributions by camera/predator inclination, θ_C, with specific angular intervals of red: $-2.4° < \theta_C \leq 10°$, orange: $-3.4° < \theta_C \leq -2.4°$, light green: $-5.6° < \theta_C \leq -3.4°$, green: $-14.9° < \theta_C \leq -5.6°$, light blue: $-26.8° < \theta_C \leq -14.9°$, and blue: $-39.8° < \theta_C \leq -26.8°$. (**C**) Contrast distributions by solar angle, θ_S, with specific bins representing red: $38° < \theta_S \leq 44.4°$; orange: $44.4° < \theta_S \leq 50.8°$, light green: $50.8° < \theta_S \leq 54°$, green: $54° < \theta_S \leq 57.2°$, light blue: $57.2° < \theta_S \leq 63.6°$, and blue: $63.6° < \theta_S \leq 70°$. (**D**) Contrast distributions by azimuth, ψ, the predator viewing angle relative to the Sun, with the specific intervals representing red: $0° < \psi \leq 60°$, orange: $60° < \psi \leq 120°$, light green: $120° < \psi \leq 180°$, green: $180° < \psi \leq 240$, light blue: $240° < \psi \leq 300°$, and blue: $300° < \psi \leq 360°$.

devices [e.g., "invisibility cloaks" (*25*)] that camouflage well for specific tasks but suffer limitations in more complex natural environments. As sensor technology extends beyond the relatively limited range of human sensory physiology and begins to fully capture nature's complexity (e.g., polarization-sensitive satellites), we should turn to natural systems for new materials and the means to use them effectively.

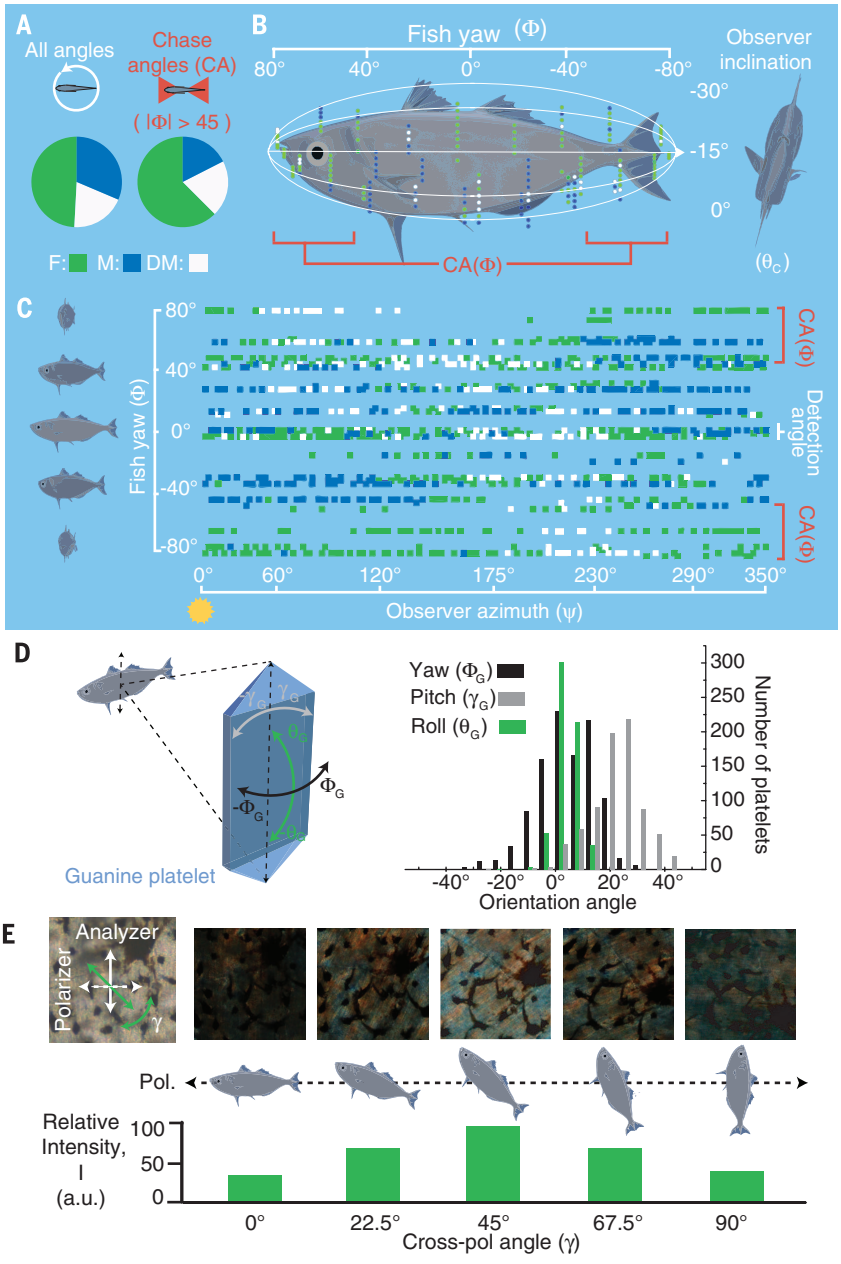

Fig. 4. Angular crypsis performance of bigeye scad in nature and in the laboratory. (**A**) Proportional crypsis performance (lowest *S*) for each surface reflector [F, bigeye scad (green); DM, diffuse mirror (white); and M, mirror (blue)] across all field measurement angles and chase angles only in the polarimeter's blue channel (a 470-nm peak). (B) and (C) The best-performing surface (lowest *S*) at measurements collected across (**B**) relative fish yaw and observer inclination angle [chase angles (CA) are noted] and (**C**) relative fish yaw and observer azimuth angles, with ψ = 0° representing the observer facing the Sun (for other contrast distributions, see fig. S3, and for model comparisons, see fig. S7). (**D**) Angular distributions of guanine platelet from three orientations (yaw, pitch, and roll) quantified from SEM measurements of bigeye scad skin, as in (*16*). (**E**) Cross-polarization light microscopy measurements of iridophore layers (collected from sagittal cross sections rotated in cross-polarization microscopy). The intensity of iridophore layers when rotated about the viewing axis between cross polarizers (linear polarizer and analyzer) produces angular (γ) dependent intensity with a maxima at 45°.

REFERENCES AND NOTES

1. A. Morel, K. J. Voss, B. Gentili, *J. Geophys. Res. C* **100**, 13143–13150 (1995).
2. E. J. Denton, *Proc. R. Soc. London Ser. B* **258**, 285–313 (1970).
3. N. J. Marshall, S. Johnsen, in *Animal Camouflage: Mechanisms and Function*, M. Stevens, S. Merilaita, Eds. (Cambridge Univ. Press, Cambridge, 2011), pp. 186–211.
4. S. Johnsen, *Integr. Comp. Biol.* **43**, 580–590 (2003).
5. S. Johnsen, *Annu. Rev. Mar. Sci.* **6**, 369–392 (2014).
6. N. W. Pankhurst, J. N. Lythgoe, *J. Fish Biol.* **21**, 279–296 (1982).
7. T. W. Cronin, N. Shashar, *J. Exp. Biol.* **204**, 2461–2467 (2001).
8. S. Sabbah, A. Lerner, C. Erlick, N. Shashar, in *Recent Research Developments in Experimental & Theoretical Biology*, S. G. Pandalai, Ed. (Transworld Research Network, Trivandrum, Kerala, India, 2005), pp. 123–176.
9. T. H. Waterman, *Biol. Rev. Camb. Philos. Soc.* **81**, 111–115 (2006).
10. S. Sabbah, N. Shashar, *J. Opt. Soc. Am. A Opt. Image Sci. Vis.* **24**, 2049–2056 (2007).
11. Y. You *et al.*, *Appl. Opt.* **50**, 4873–4893 (2011).
12. P. C. Brady, K. A. Travis, T. Maginnis, M. E. Cummings, *Proc. Natl. Acad. Sci. U.S.A.* **110**, 9764–9769 (2013).
13. N. W. Roberts, M. L. Porter, T. W. Cronin, *Proc. Phys. Soc. London. Sect. B* **366**, 627 (2011).
14. M. Kamermans, C. W. Hawryshyn, *Proc. Phys. Soc. Lond. Sect. B* **366**, 742 (2011).
15. G. M. Calabrese, P. C. Brady, V. Gruev, M. E. Cummings, *Proc. Natl. Acad. Sci. U.S.A.* **111**, 13397–13402 (2014).
16. S. Zhao, P.C. Brady, M. Gao, R. Etheredge, G. Kattawar, M. Cummings, *J. R. Soc. Interface* **12**, 10.1098/rsif.2014.1390 (2015).
17. T. Jordan, J. Partridge, N. Roberts, *Nat. Photon.* **6**, 759–763 (2012).
18. A. A. Gilerson *et al.*, *Appl. Opt.* **52**, 8685–8705 (2013).
19. Y. You *et al.*, *J. Geophys. Res. Oceans* **116**, C00H05 (2011).
20. J. K. Parrish, *Environ. Biol. Fishes* **34**, 257–263 (1992).
21. M. J. Cermak, *Biol. Bull.* **203**, 241–243 (2002).
22. N. O. Handegard *et al.*, *Curr. Biol.* **22**, 1213–1217 (2012).
23. J. Haag, J.S. Jaffe, A. M. Sweeney, *Opt. Exp.* **21**, 3603–3616 (2013).
24. S. Johnsen, E. Gassmann, R. A. Reynolds, D. Stramski, C. Mobley, *Limnol. Oceanogr.* **59**, 1839–1852 (2014).
25. R. Schittny, M. Kadic, T. Bückmann, M. Wegener, *Science* **345**, 427–420 (2014).

ACKNOWLEDGMENTS

All experiments were approved by the University of Texas animal care committee (under Institutional Animal Care and Use Committee protocols AUP-2009-00022 and AUP-2015-00026). This research was supported by Office of Naval Research Multi-University Research Initiative grant N000140911054 to M.E.C., H.M.D., J.S., A.A.G., and G.W.K.; and NSF Division of Ocean Sciences grant 1130793 to M.E.C. and G.W.K. The data are deposited though the Dryad Digital Repository (10.5061/dryad.gt37j).

SUPPLEMENTARY MATERIALS

www.sciencemag.org/content/350/6263/965/suppl/DC1
Materials and Methods S1 to S5
Figs. S1 to S7
Tables S1 to S10
References (*26–39*)

26 September 2015; accepted 19 October 2015
10.1126/science.aad5284

Open-ocean fish reveal an omnidirectional solution to camouflage in polarized environments

Parrish C. Brady *et al.*

Science **350**, 965 (2015);
DOI: 10.1126/science.aad5284